DIAGNOSING CLEFT LIP PATHOLOGY IN 3D ULTRASOUND: A LANDMARKING-BASED APPROACH

DIAGNOSING CLEFT LIP PATHOLOGY IN 3D ULTRASOUND: A LANDMARKING-BASED APPROACH

Enrico Vezzetti[1], Domenico Speranza[2], Federica Marcolin[1], and Giulia Fracastoro[1]

[1]Department of Management and Production Engineering, Politecnico di Torino, Italy; [2]Dipartimento di Ingegneria Civile e Meccanica, Università degli Studi di Cassino e del Lazio Meridionale, Italy
e-mails: enrico.vezzetti@polito.it; d.speranza@unicas.it; federica.marcolin@polito.it; giulia.fracastoro@studenti.polito.it

ABSTRACT

Aim of this work is to automatically diagnose and formalize prenatal cleft lip with representative key points and identify the type of defect (unilateral, bilateral, right, or left) in three-dimensional ultrasonography (3D US). Differential Geometry has been used as a framework for describing facial shapes and curvatures. Then, descriptors coming from this field are employed for identifying the typical key points of the defect and its dimensions. The descriptive accurateness of these descriptors have allowed us to automatically extract reference points, quantitative distances, labial profiles, and to provide information about facial asymmetry. Eighteen foetal faces, ten of healthy foetuses and eight with different types of cleft lips, have been obtained through a Voluson system and used for testing the algorithm. Cleft lip has been diagnosed and correctly characterized in all cases. Transverse and cranio-caudal length of the cleft have been computed and upper lip profile has been automatically extract to have a visual quantification of the overall labial defect. The asymmetry information obtained is consistent with the defect. This algorithm has been designed to support practitioners in identifying and classifying cleft lips. The gained results have shown that Differential Geometry might be a proper tool for describing faces and for diagnosis.

Keywords: Cleft lip; dysmorphisms; landmarking; syndrome diagnosis; 3D ultrasound.

INTRODUCTION

Three-dimensional ultrasound (US) has been introduced more than twenty years ago into clinical practice (Riccabona *et al.*, 1997). Its applications on diagnosis of anomalies and diseases were a direct consequence of its use. In particular, cleft lip and palate (CLP) detection, whose incidence is 1/700 in United States (Tonni and Lituania, 2013), was widely addressed, as they could be difficult to be diagnosed with bi-dimensional US, especially in earlier gestational ages (Hata *et al.*, 1998). In the effort to quantify the performance of routine ultrasonographic screening on an unselected population, the Eurofetus study (Grandjean *et al.,* 1999) shows that CLP has the lowest rates of detection (18%) and it is diagnosed usually later in pregnancy (only 31.6% before 24 weeks). Furthermore, CLP is identified with a lower occurrence by prenatal US when the anomaly is isolated than in the cases where multiple anomalies coexist, as frequently noticed during autopsies following termination of pregnancy of foetuses with diagnosed multiple diseases (Luck *et al.,* 1992). Complementarily, 3D, despite some criticisms (Maarse *et al.*, 2010), has been considered more accurate than bi-dimensional data in detecting unaffected lips at less than 24 weeks (Pretorius *et al.*, 1995).

In this work we will focus on cleft lip (CL) alone. CL, "both unilateral and bilateral, includes clefts involving the alveolus and hard palate anterior to the incisive foramen, namely the embryological primary palate" (Demircioglu *et al.*, 2008). The tested rates of antenatal detection of CL range 21-30% (Rotten and Levaillant, 2004).

Cleft lip has been associated with more than one-hundred different chromosomal abnormalities and genetic syndromes (Jones, 1993), and sometimes may be the only sign of a chromosomal anomaly, as trisomy 18 (Carlson, 2000), trisomy 13, or syndromes such as Cornelia de Lange or Smith-Lemli–Opitz (Roelfsema *et al.*, 2007). Thus, an accurate scan searching for other foetal anomalies and a genetic counselling are paramount when a cleft lip is diagnosed. Cleft lip does not go with any palatal abnormality in 15-25% cases (Bäumler *et al.*, 2011, Offerdal *et al.,* 2008). More generally, if we consider CLP as a whole, the incidence of structural anomalies and syndromes accompanying cleft lip and palate ranges between 21% and 38% (Campbell *et al.*, 2005). But it is important to note that, although they often occur with each other, cleft lip and palate abnormalities are "developmentally distinct processes" (Lee *et al.*, 2000). In particular, the embryological origins of lips and alveolus clefts appear to be distinct from those of secondary palate cleft (Campbell *et al.*, 2005).

Lee *et al.* (2000) used three-dimensional ultrasonography to support cleft lip and palate detection. CL was identified by an examiner as "a loss of continuity of the orbicularis oris muscle from a coronal or axial view of the lips" (Lee *et al.*, 2000), so the diagnosis was not automatic. Campbell *et al.* (2005) assessed the clinical value of a three-dimensional US technique, the 'reverse face' view, in the prenatal categorization of orofacial clefts including CL. Then, Platt *et al.* (2006) proposed the 'flipped face' view to diagnose lip and palate cleftings, relying on 3D US. When a static volume is acquired, it is rotated 90° so that the cut plane is directed in a chin-to-nose plane and scrolled to examine in sequential order different zones, including lips. Mailáth-Pokorny *et al.* (2010) investigated the role of foetal MRI in the antenatal diagnosis of facial clefts, including cleft lip, although no particular detection technique has been employed. Martinez-Ten *et al.* (2012) investigated whether systematic examination of primary and secondary palate supported the detection of face cleftings during first trimester. Gindes *et al.* (2013) studied the potential of three-dimensional US for palate view in foetuses at high risk for CLP. An in-depth palate assessment was made adopting both 2D and 3D US on the axial plane. Then, the outcoming prenatal diagnosis was compared to after-birth findings.

Some authors used landmarks as reference points. Johnson *et al.* (2000) assessed the advantages of three-dimensional US in diagnosing cleft lip. The volume data were displayed in two formats: three orthogonal planar images and a three-dimensional rendered image of the foetal facial surface. The planar images were "rotated with the interactive display into a standard anatomic orientation, so that the three planar images corresponded to the frontal, sagittal, and transverse facial planes" (Johnson *et al.*, 2000). The rendered image provided landmarks for the planar images. Roelfsema *et al.* (2007) used 3D US to perform foetal orofacial clefts examination and quantified the craniofacial variability index (CVI) in distinguishing between isolated cleft lip/palate and cleft lip/palate in chromosomal abnormalities or syndromes. Facial landmarks such as tragus, nasion, gnathion, glabella, subnasion, and others were employed to extract sixteen craniofacial measurements for the evaluation of after-birth abnormal/regular orofacial development. Although none of the foetuses evaluated in their study was affected by cleft lip, Sepulveda *et al.* (2010) proposed a novel sonographic landmark typical of the first trimester, the 'retronasal triangle', to be adopted for the early screening of CP. This landmark has been termed this way because coronal plane displays three easily identifiable echogenic lines: the two maxilla frontal processes and the primary palate. Manganaro *et al.* (2011) studied CLP via MRI and ultrasound, although not 3D. Facial landmarks in the zones of forehead, occiput, orbits, nose, lips, chin, mandible were identified and analyzed for each foetus. Tonni and Lituania (2012) proposed a new three-dimensional sonographic software, the OmiView algorithm, and applied it to unilateral CL, bilateral CLP, and isolated CP. They showed that 3D imaging of the foetal hard and soft palates by OmniView was technically easier than with previously reported 3D techniques. OmniView allowed visualization of all anatomical landmarks of the specific targeted zone, i.e. labia, primary palate, alveolar ridge, posterior palate, uvula, velum, and tongue.

This work introduces a methodology for automatically diagnosing cleft lip and assessing specific information about the detected cleft, such as transverse and cranio-caudal lengths, upper lip outline, and a quantification of facial asymmetry.

MATERIALS AND METHODS

During 2013, 38 3D volumes of 38 foetuses at 22-32 weeks' gestation were acquired. Eight of them were foetuses affected by cleft lip. Written informed consent was obtained from the parents for publication of clinical details, clinical images, and videos. Principles outlined in the Declaration of Helsinki have been followed.

Among these acquisitions, 18 were selected and processed for the purposes of the study, keeping all the eight faces with cleft lip. The leftover ones were excluded due to damages, acquisition inaccuracy, noise, and wrong or unusable foetus's position, such as hands on face or similar.

The US equipment was a Voluson system (GE Healthcare, Wauwatosa, WI, USA), with a RAB 4-8 (real time 4D convex transducer probe). The GE RAB 4-8 has a frequency range of 4 to 8 MHz and is used for OB applications (Footprint 63.6 x 37.8 mm, FOV 70°, V 85°x70°). Table 1 shows data details and respective scan settings.

Ultrasound examination											
Volume Ultrasound: GE Voluson e - Transducer: RAB 4-8-RS/OB											
Foetus		**Scan Setting**									**Defect**
Name	**Week**	**MI**	**Fr**	**TIs**	**Quality**	**Th**	**B(°)**	**V(°)**	**Mix**	**SRI**	**Cleft lip?**
Anto	32	0,9	4,2/10,8 cm/51 Hz	0,1	max	30	52	65	40/60	II	no
Bart	32	0,9	3,7/11,0 cm/52 Hz	0,1	max	29	50	65	50/50	II	no
Lisa	32	1,	4,1/9,7 cm/54	0,	max	3	53	65	40/6	II	no

		1	Hz	1		0			0		
Gio	22	1,1	3,6/10,2 cm/58 Hz	0,1	max	30	47	65	40/60	II	no
Gian	22	1,0	3,6/8,1 cm/68 Hz	0,1	high 2	30	46	65	40/60	II	no
Paul	32	1,1	2,8/10,9 cm/49 Hz	0,2	max	30	54	65	40/60	II	no
Pie	32	1,1	1,7/8,1 cm/55 Hz	0,1	max	30	58	65	40/60	II	no
Elena	32	0,9	4,2/10,8 cm/47 Hz	0,1	max	30	56	65	40/60	II	no
Fede	32	0,9	4,4/11,1 cm/51 Hz	0,1	max	30	50	65	40/60	II	no
Simon	32	1,1	3,5/9,6 cm/56 Hz	0,1	max	30	50	65	40/60	II	no
A	32	0,9	4,2/10,8 cm/51 Hz	0,1	max	30	52	65	40/60	II	Unilateral complete
B	32	0,9	3,7/11,0 cm/52 Hz	0,1	max	29	50	65	50/50	II	Unilateral complete
C	32	0,9	4,2/10,8 cm/47 Hz	0,1	max	30	56	65	40/60	II	Bilateral complete
D	32	0,9	4,4/11,1 cm/51 Hz	0,1	max	30	50	65	40/60	II	Bilateral complete
E	22	1,0	3,6/8,1 cm/68 Hz	0,1	high 2	30	46	65	40/60	II	Unilateral incomplete
F	32	1,1	4,1/9,7 cm/54 Hz	0,1	max	30	53	65	40/60	II	Unilateral incomplete
G	32	1,1	2,8/10,9 cm/49 Hz	0,2	max	30	54	65	40/60	II	Unilateral complete
H	32	1,1	3,5/9,6 cm/56 Hz	0,1	max	30	50	65	40/60	II	Unilateral incomplete

Table 1. Weeks' gestation, scan settings, and eventual cleft lip features for each baby.

4D VIEW software allows to see the acquired images on three orthogonal planes: axial, sagittal, and coronal (Fig. 1, above). The plane chosen for the facial shell modelling is the midsagittal (Fig. 1, below).

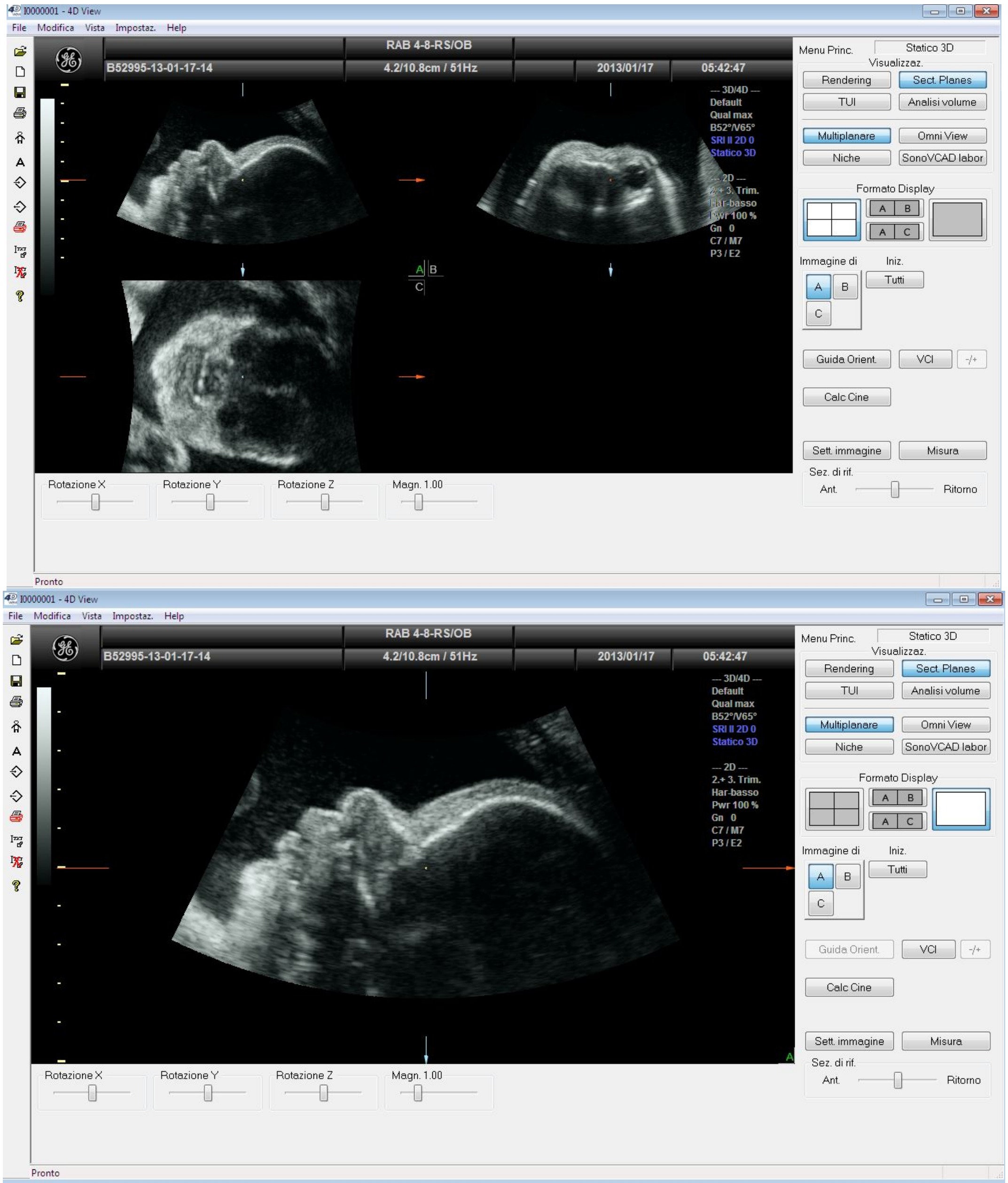

Figure 1. Multiplanar image (above) and midsagittal plane (below).

The distance between two successive slices is 0.4 mm. For each slice composing the whole facial volume, the relative DICOM format file is generated and imported into Simpleware ScanIP software for the three-dimensional model reconstruction. Facial data were collected in point clouds (shells), imported in Matlab®, triangulated, and converted into a squared-grid-based depth map.

The algorithm we developed for foetal diagnosis of cleft lip was elaborated, implemented, and run on these shells. It relies on the geometrical features of foetus's face in order to detect the deformation. Moreover, the algorithm identifies whether the cleft lip is unilateral or bilateral, localizes some key points of the deformation and performs tailored measurements in order to assess cleft quantification. The upper lip outline is also evaluated, in order to provide shape and size description of the defect. The geometrical descriptors used in this work are defined and described in the Appendix. These descriptors rely on previous work of our research group (Calignano and Vezzetti, 2010; Vezzetti *et al.*, 2011-2014). Figures 2-8 show their behaviour on a facial shell with cleft lip.

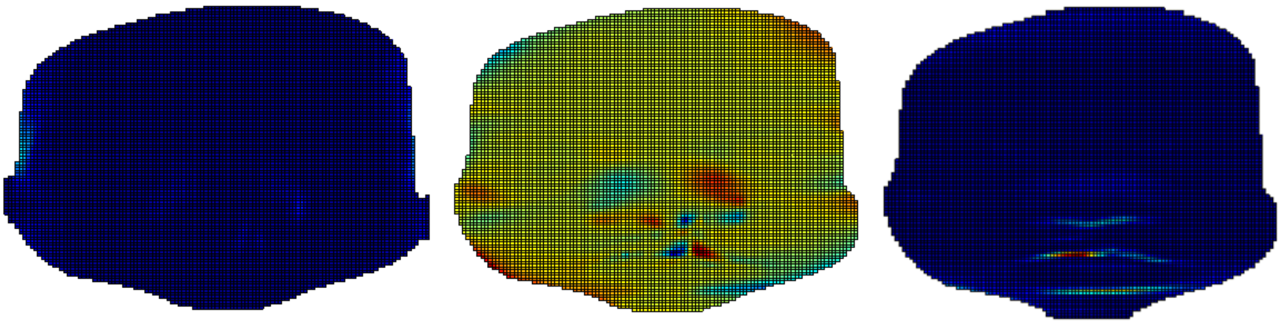

Figure 2. The coefficients of the first fundamental form *E*, *F* and *G*.

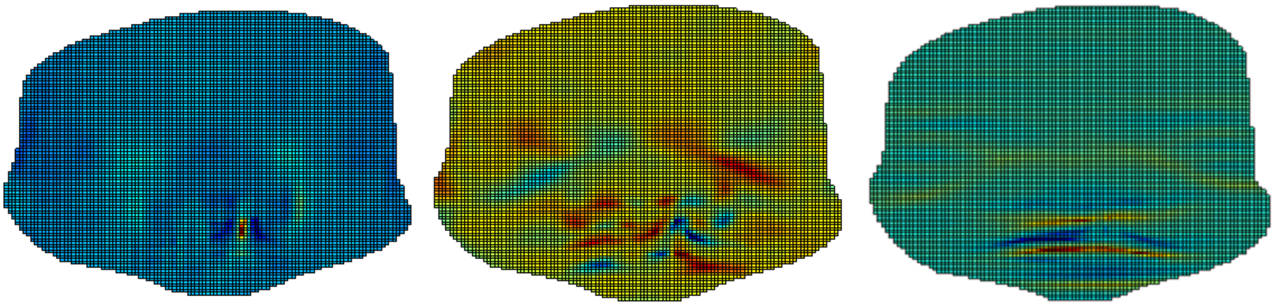

Figure 3. The coefficients of the second fundamental form *e*, *f* and *g*.

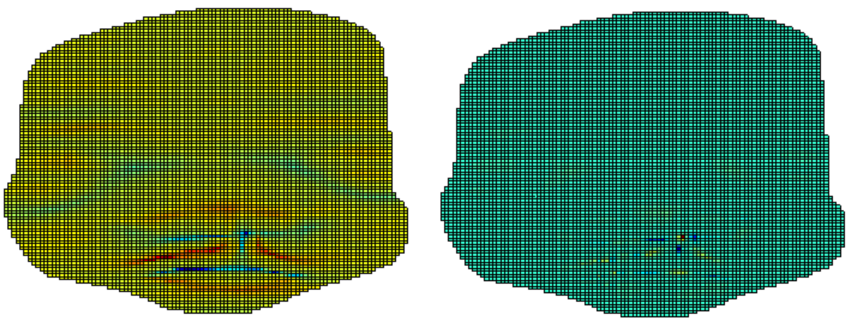

Figure 4. The mean and Gaussian curvature *H* and *K*.

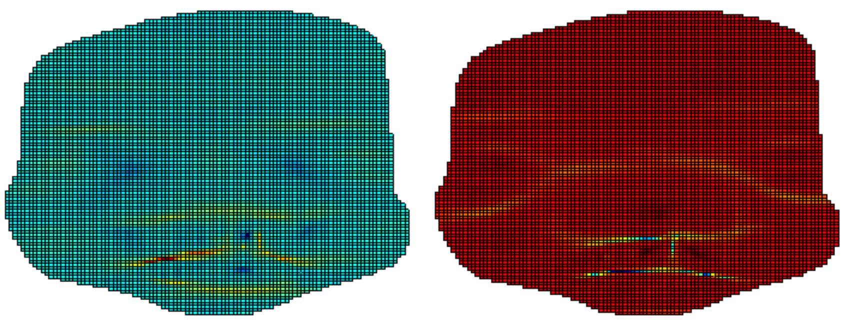

Figure 5. The principal curvatures k_1 and k_2.

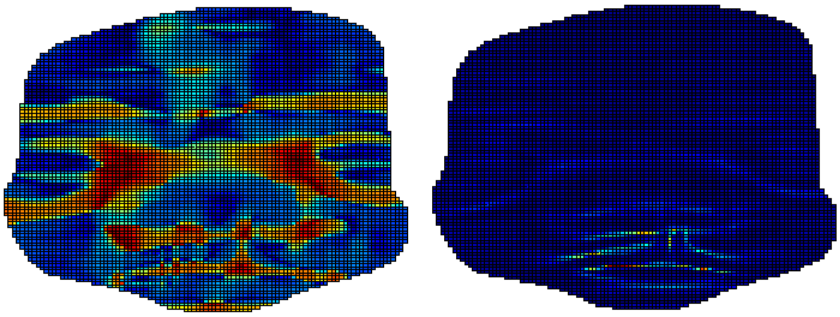

Figure 6. The Shape and Curvature Indexes *S* and *C*.

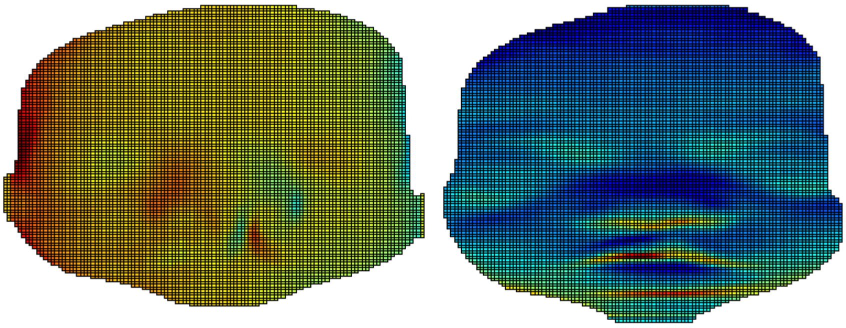

Figure 7. The first derivatives *Dx* and *Dy*.

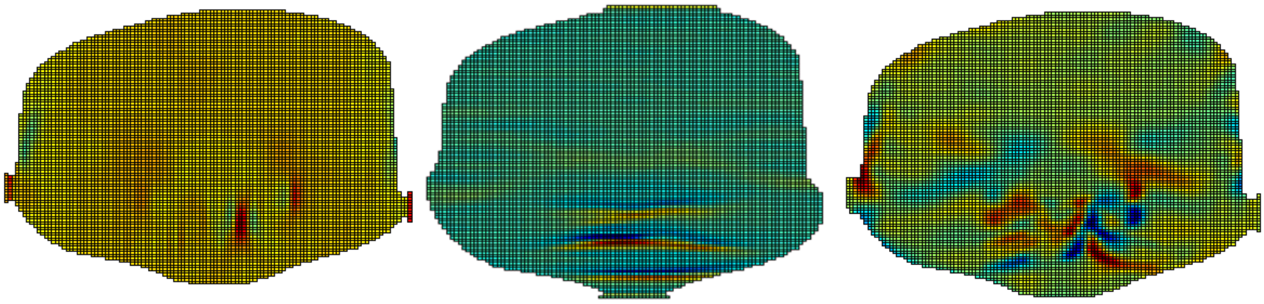

Figure 8. The second derivatives *Dxx*, *Dyy* and *Dxy*.

DETECTION OF THE DEFORMITY

Cleft lip is a gap/indentation in the upper lip. The proposed algorithm demonstrates that this defect could be detected via point-by-point mapping geometrical descriptors on facial depth map. This indentation is characterized by high numerical values of coefficient *e* and of Curvedness Index *C* in correspondence to the zone of interest, as shown in Figure 9. Moreover, the two parts of the lip that are located beside the indentation are characterized by two maximums of the principal curvature k_2, as can be seen in Figure 10.

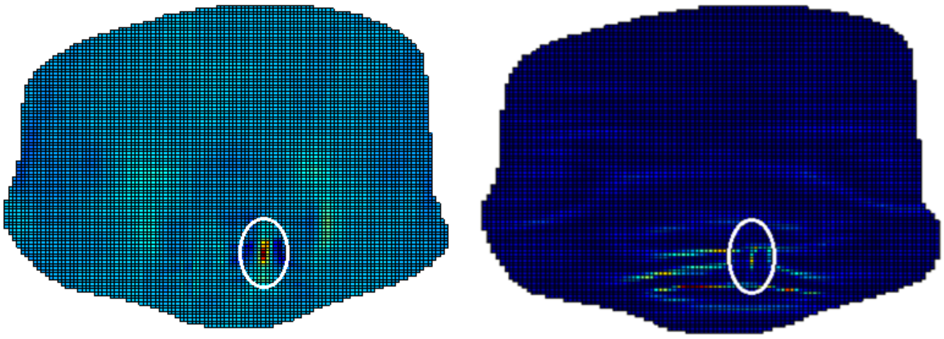

Figure 9. The behaviour of the coefficient *e* (left) and of the Curvedness Index *C* (right) in a foetus with cleft lip. The circle highlights the area of the gap.

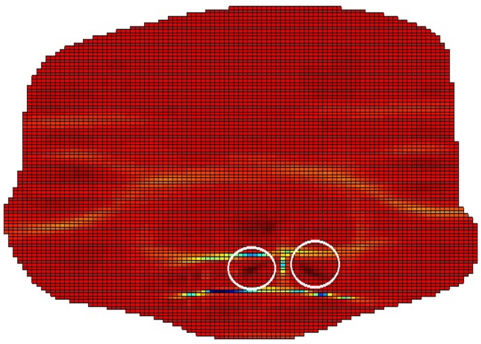

Figure 10. The behaviour of the principal curvature k_2 in a foetus with cleft lip. The two circles highlight the areas of the lip beside the gap.

The designed algorithm adopts the previous geometrical features to detect whether the cleft lip is present or not in a foetus's face. Moreover, this algorithm is able to automatically distinguish between unilateral and bilateral cleft lip. It is composed by the following steps.

1. The algorithm searches if there are points whose coefficient *e* and Curvedness Index *C* are greater than a threshold value ($C>3$ and $e>3.5$). These are the geometrical features of the gap in the lip. Thresholds are set via experimentation.
2. If the search of the step 1 gives no results, the cleft lip is not present. Otherwise, another check is performed in order to verify that a cleft lip is really present. For each point that satisfies the conditions of step 1, the algorithm searches if in its neighbourhood there are points with a high value of the principal curvature k_2 ($k_2>0.3$). These are the geometrical features of the two parts of the lip beside the gap. This further condition is needed, as in some

cases the points close to the *alae* of the nose could have the same geometrical features searched in step 1.

3. If the search of the previous step gives no results, the cleft lip is not present; otherwise it is.
4. In order to verify if it is an unilateral or bilateral cleft lip, the algorithm checks if the points that satisfy the condition of step 1 and 2 are all in the same neighbourhood or not. If they do not belong to the same neighbourhood, the cleft lip is bilateral.

The steps of the process are explained in the scheme of Figure 11.

In Figure 12, the points found in step 1 and 2 are shown in a shell with an unilateral cleft lip.

In Figure 13, the points found in step 1 and 2 are shown in a shell with a bilateral cleft lip.

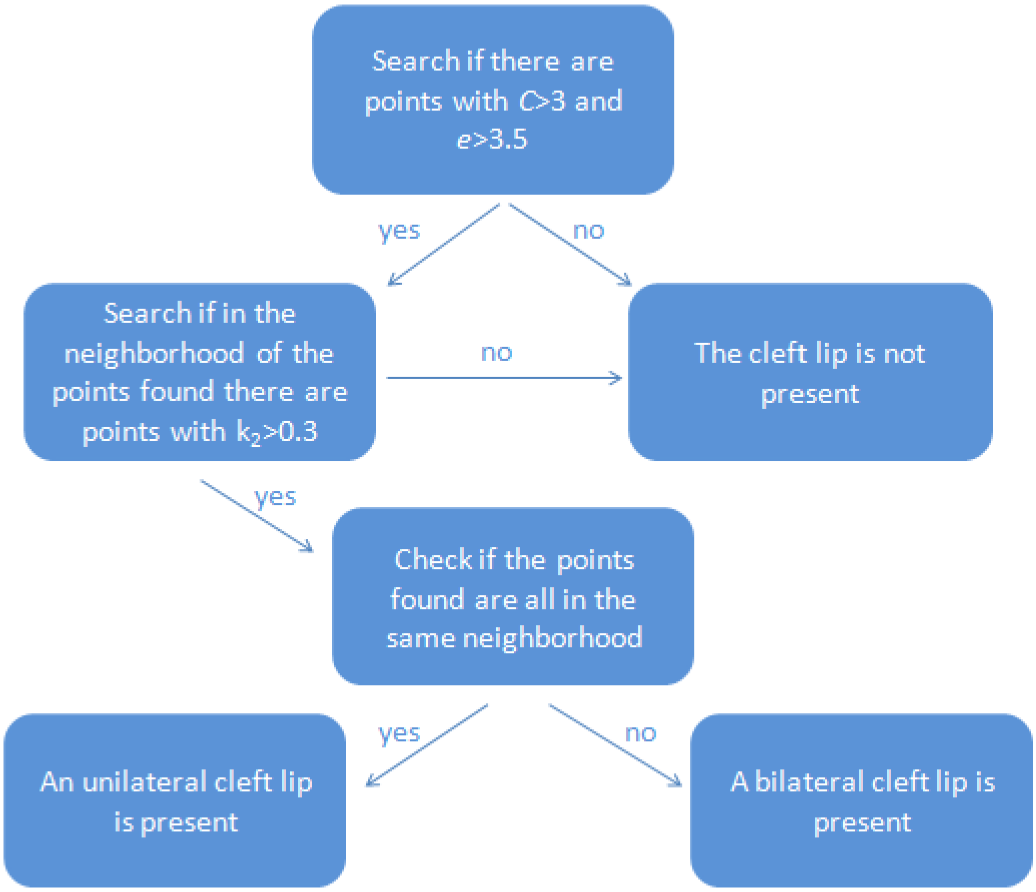

Figure 11. Scheme of the process for cleft lip diagnosis.

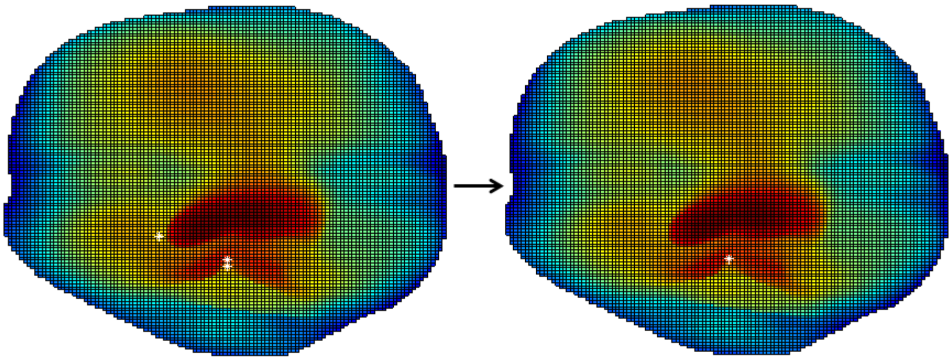

Figure 12. On the left: the points found in the first step of the algorithm. On the right: the points found in the second step of the algorithm.

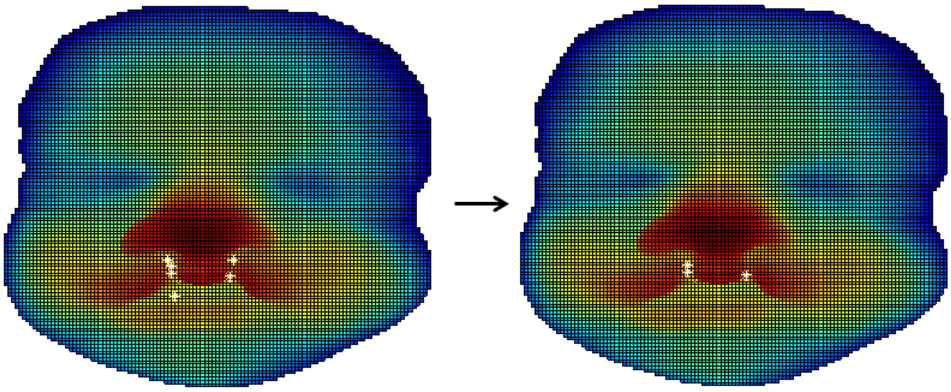

Figure 13. On the left: the points found in the first step of the algorithm. On the right: the points found in the second step of the algorithm.

LOCALIZATION OF KEY POINTS

In order to quantify the deformation, four key points are automatically localized: the two points of the lip that are beside the cleft and the ending points of the cleft, shown in Figure 14.

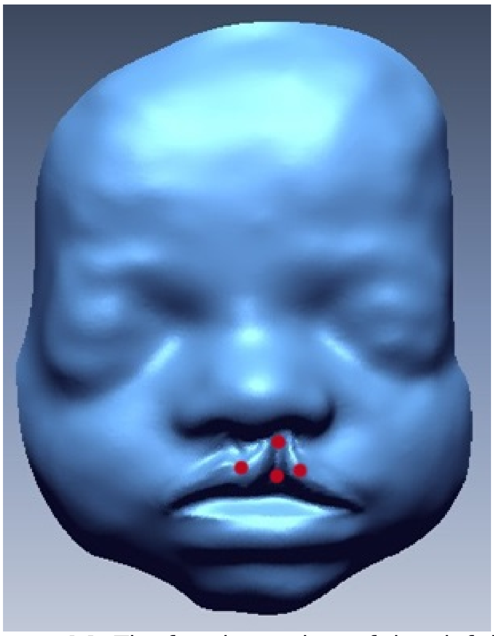

Figure 14. The four key points of the cleft lip.

As mentioned above, the principal curvature k_2 has two maximums in the first two points. The automatic localization algorithm:

1. after deformity detection, identifies two regions in the neighbourhood of the cleft, one on the right side and one on the left side;
2. in each region, selects the points with $D_y<0$;
3. maximizes the principal curvature k_2.

The other two points are located in the gap of the lip. As said above, this area is characterized by high values of the Curvedness Index *C* and of coefficient *e*. To extract these points, firstly the algorithm localizes the centre of the cleft maximizing the coefficient *e*. Then, it analyzes the neighbourhood of this point, moving upwards from the centre to the high ending point and downwards till the low ending point. The algorithm, for each *y* value, maximizes the coefficient *e* in a neighbourhood of the cleft lip. The ending points are the first two maximums that are lower than a proper threshold value, established via experimentation.

MEASUREMENT OF THE DEFORMATION AND EXTRACTION OF THE UPPER LIP OUTLINE

Transverse diameter of the cleft was evaluated by computing the Euclidean distance between the first two points extracted; its cranio-caudal length by computing the Euclidean distance between the last two points extracted. These two distances, represented in Figure 15, are the most adopted in the estimation of cleft size.

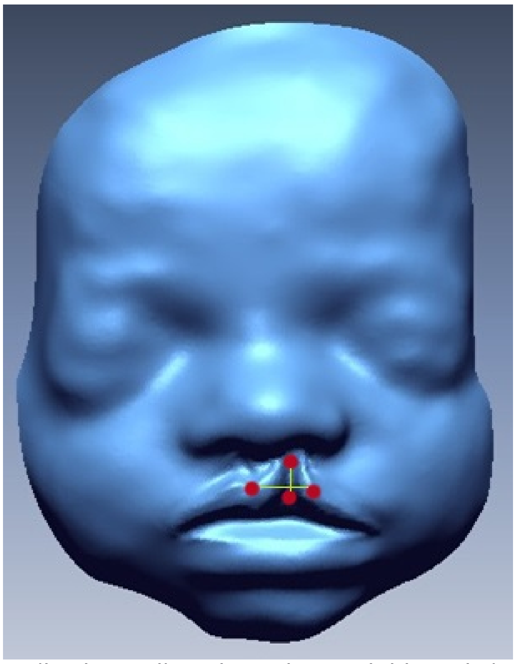

Figure 15. The transverse (horizontal) and cranio-caudal length (vertical) of the cleft.

The outline of the upper lip was also extracted, in order to provide an extra information about its shape. The Curvedness Index was adopted, as it is one of the geometrical descriptors that more accurately highlights upper lip surface behaviour. As shown in Figure 16, the Curvedness Index has a maximum behaviour in correspondence to the upper lip. To extract the outline, for each *x* value in the upper lip area, the Curvedness Index is maximized. This way, we obtain a sequence of points, namely a line, in the 3D space that describes the upper lip area.

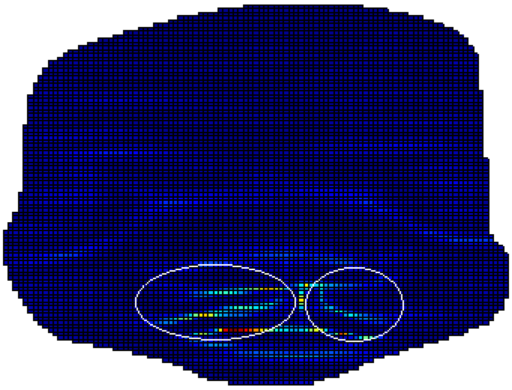

Figure 16. The Curvedness Index. The two circles highlight the upper lip area.

EVALUATION OF FACE ASYMMETRY

Facial asymmetry was also evaluated in the cases of unilateral cleft lip. To perform this evaluation, the mean of the absolute value of the coefficient *e* was computed in both left and right parts of the mouth. By comparing these two mean values, we obtain an useful information about the asymmetry of the face. Coefficient *e* is chosen and its absolute value is taken, as in correspondence of the cleft lip two minimums and a maximum are present (as it was previously shown in Figure 8); the absolute value will avoid that the minimum and maximum behaviour will annul each other when the mean area is computed.

RESULTS AND DISCUSSION

The algorithm for the diagnosis of cleft lip was tested on the eighteen ultrasounds (eight with cleft lip and ten without). In all these cases, the algorithm correctly detected the presence/absence of the cleft and, in the two shells with bilateral cleft lip, the algorithm detected both the clefts.

In the eight ultrasounds with cleft lip, the four key points were localized. In Figure 17 the resulting four key points are shown for each shell.

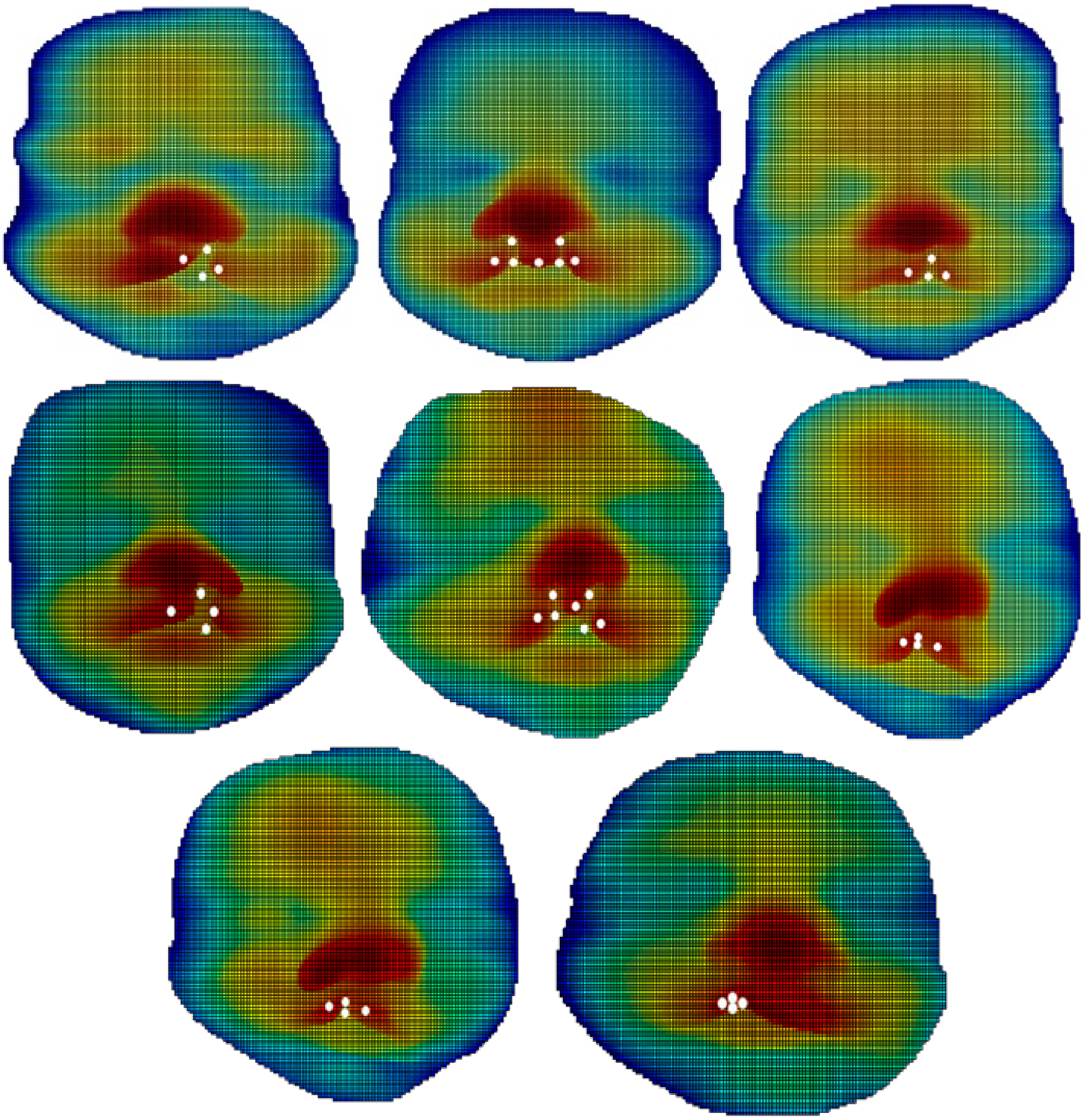

Figure 17. The resulting four key points for each shell with cleft lip.

After having localized the four key points, transverse and the cranio-caudal length are computed. In Table 2, the values of these distances for each shell are shown. The unit of measurement is the millimetre. As can be seen, the shells that present the lowest cranio-caudal length are the ones with an incomplete cleft.

A	7.19	6.78
B	8.31	9.59
C (left cleft)	15.08	7.00
C (right cleft)	12.04	7.06
D (left cleft)	12.65	6.09
D (right cleft)	10.01	12.34

E	6.69	1.81
F	6.67	1.64
G	6.19	4.34
H	3.17	0.62

Table 2. Computed distances for each shell.

For each shell with cleft lip, upper lip outline was extracted. Results are shown in Figure 18.

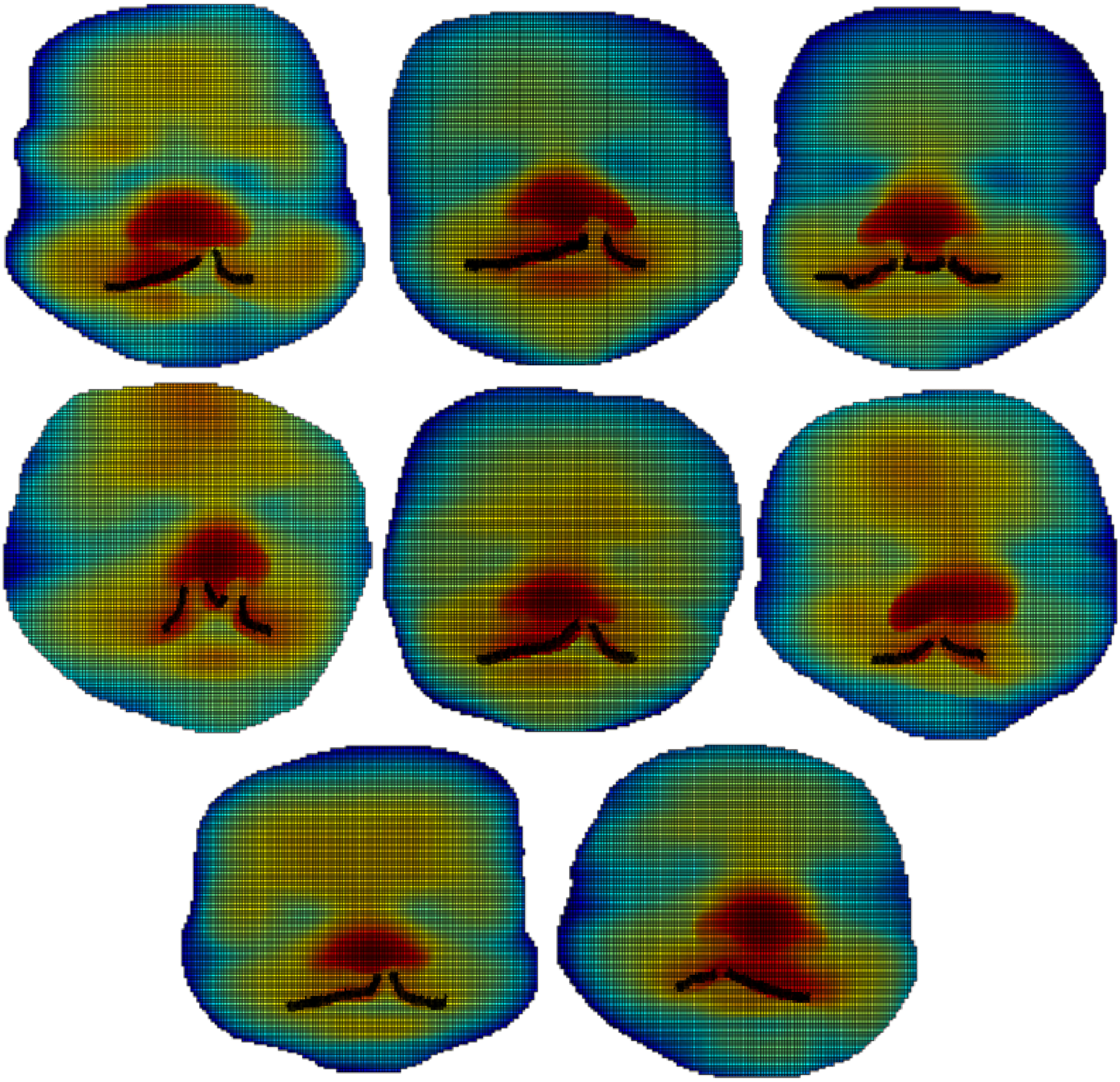

Figure 18. The resulting upper lip outline for each shell with cleft lip.

We computed facial asymmetry in the six shells with unilateral cleft lip and on the ten shells without cleft lip; the evaluation was not performed on the two shells with bilateral cleft lip. The results are shown in Table 3 (shells with unilateral cleft lip) and 4 (shells without cleft lip).

Shell	Side with cleft lip	Side without cleft lip	Difference
A	1.08	0.41	0.68
B	1.34	0.4	0.94
E	1.10	0.36	0.74
F	0.82	0.60	0.22
G	1.09	0.33	0.76
H	0.44	0.28	0.16

Table 3. Results of asymmetry evaluation for shells with unilateral cleft lip.

Shell	Left side	Right side	Difference
Anto	0.28	0.33	0.05
Bart	0.30	0.48	0.18
Elena	0.16	0.27	0.11
Fede	0.33	0.30	0.03
Gian	0.22	0.33	0.11
Gio	0.16	0.24	0.08
Lisa	0.36	0.21	0.14
Paul	0.17	0.22	0.05
Pie	0.15	0.20	0.05
Simon	0.18	0.25	0.07

Table 4. Results of asymmetry evaluation for shells without cleft lip.

As can be seen in Tables 3 and 4, the difference between the two sides of the face is usually higher in the shells with cleft lip. The mean difference value is 0.58 mm in shells with cleft lip instead it is 0.09 mm in shells without cleft lip, i.e. about six times smaller. The shell with cleft lip with the lowest difference value is H, where an incomplete cleft lip is present. Probably in this case the asymmetry was not high because the cleft lip was not accentuated, as can be verified in Table 2, where the shell H has the lowest cranio-caudal length. Also, the other shell with a low difference value, namely shell E, presents an incomplete cleft lip. Instead, in the shells without cleft lip the difference between the two face sides is usually low, with values ranging between 0.05 and 0.18 millimetres. The highest values (Bart and Lisa) are probably due to the quality of the ultrasound.

CONCLUSIONS

This work presents a new algorithm for diagnosing cleft lip on 3D ultrasound. The proposed algorithm was developed with Matlab® and tested on eighteen foetuses' faces (eight with cleft lip and ten healthy). The algorithm automatically states whether the defect is present or not, classifies it (unilateral, bilateral, right, left), extracts four key points, transverse and cranio-caudal length of the cleft, and upper lip outline, and provides information on the facial asymmetry. The defect has been correctly diagnosed and classified for all the foetuses.

Differential Geometry provided us with a set of descriptors leading this research activity. The result is that these descriptors are suitable to describe facial shape and curvedness, allowing an accurate extraction of the interested facial features.

ACKNOWLEDGEMENT

The authors declare that they have no conflicts of interest to disclose.

REFERENCES

Bäumler M, Faure JM, Bigorre M, Bäumler-Patris C, Boulot P, Demattei C, Captier G (2011). Accuracy of prenatal three-dimensional ultrasound in the diagnosis of cleft hard palate when cleft lip is present. Ultrasound Obstet Gynecol 38:440–444.

Calignano F, Vezzetti E (2010). Soft tissue diagnosis in maxillofacial surgery: a preliminary study on three-dimensional face geometrical features-based analysis. Aesthetic plastic surgery 34(2):200-11.

Campbell S, Lees C, Moscoso G, Hall P (2005). Ultrasound antenatal diagnosis of cleft palate by a new technique: the 3D 'reverse face' view. Ultrasound Obstet Gynecol 25:12-18.

Carlson DE (2000). Opinion — The ultrasound evaluation of cleft lip and palate—a clear winner for 3D. Ultrasound Obstet Gynecol 16:299-301.

Demircioglu M, Kangesu L, Ismail A, Lake E, Hughes J, Wright S, Sommerlad BC (2008). Increasing accuracy of antenatal ultrasound diagnosis of cleft lip with or without cleft palate, in cases referred to the North Thames London Region. Ultrasound Obstet Gynecol 31:647–51.

Gindes l, Weissmann-Brenner A, Zajicek M, Weisz B, Shrim A, Geffen KT, Mendes D, Kuint J, Berkenstadt M, Achiron R (2013). Three-dimensional ultrasound demonstration of the fetal palate in high-risk patients: the accuracy of prenatal visualization. Prenatal Diagnosis 33:436–41.

Grandjean H, Larroque D, Levi S (1999). The performance of routine ultrasonographic screening of pregnancies in the Eurofetus Study. Am J Obstet Gynecol 181(2):446-54.

Hata T, Yonehara T, Aoki S, Manabe A, Hata K, Miyazaki K (1998). Three-Dimensional Sonographic Visualization of the Fetal Face. American Journal of Roentgenology 170(February):481-3.

Luck CA (1992). Value of routine ultrasound scanning at 19 weeks: a four year study of 8849 deliveries. BMJ 304(6840):1474-8.

Johnson DD, Pretorius DH, Budorick NE, Jones MC, Lou KV, James GM, Nelson TR (2000). Fetal Lip and Primary Palate: Three-dimensional versus Two-dimensional US. Radiology 217(1):236–9.

Jones MC (1993). Facial clefting. Etiology and developmental pathogenesis. Clin Plast Surg 20(4):599-606.

Lee W, Kirk JS, Shaheen KW, Romero R, Hodges AN, Comstock CH (2000). Fetal cleft lip and palate detection by three-dimensional ultrasonography. Ultrasound Obstet Gynecol 16:314-20.

Maarse W, Bergé SJ, Pistorius L, Van Barneveld T, Kon M, Breugem C, Mink van der Molen AB (2010). Diagnostic accuracy of transabdominal ultrasound in detecting prenatal cleft lip and palate: a systematic review. Ultrasound Obstet Gynecol 35:495–502.

Mailáth-Pokorny M, Worda C, Krampl-Bettelheim E, Watzinger F, Brugger PC, Prayers D (2010). What does magnetic resonance imaging add to the prenatal ultrasound diagnosis of facial clefts?. Ultrasound Obstet Gynecol 36:445–51.

Manganaro L, Tomei A, Fierro F, Di Maurizio M, Sollazzo P, Sergi ME, Vinci V, Bernardo S, Irimia D, Cascone P, Marini M (2011). Fetal MRI as a complement to US in the evaluation of cleft lip and palate. Radiol med 116:1134–48.

Martinez-Ten P, Adiego B, Illescas T, Bermejo C, Wong AE, Sepulveda W (2012). First-trimester diagnosis of cleft lip and palate using three-dimensional ultrasound. Ultrasound Obstet Gynecol 40:40–6.

Mittermayer C, Lee A (2003). Picture of the Month — Three-dimensional ultrasonographic imaging of cleft lip: the winners are the parents. Ultrasound in Obstetrics and Gynecology 21:628-9.

Offerdal K, Jebens N, Syvertsen T, Blaas HG, Johansen OJ, Eik-Nes SH (2008). Prenatal ultrasound detection of facial clefts: a prospective study of 49,314 deliveries in a non-selected population in Norway. Ultrasound Obstet Gynecol 31(6):639-46.

Platt LD, DeVore GR, Pretorius DH (2006). Improving Cleft Palate/Cleft Lip Antenatal Diagnosis by 3-Dimensional Sonography — The “Flipped Face” View. J Ultrasound Med 25:1423–30.

Pretorius DH, House M, Nelson TR, Hollenbach KA (1995). Evaluation of Normal and Abnormal Lips in Fetuses: Comparison Between Three- and Two-Dimensional Sonography. American Journal of Roentgenology 165(5):1233-7.

Riccabona M, Pretorius DH, Nelson TR, Johnson D, Budorick NE (1997). Three-Dimensional Ultrasound: Display Modalities in Obstetrics. J Clin Ultrasound 25(4):157–67.

Roelfsema NM, Hop WCJ, Van Adrichem LNA, Wladimiroff JW (2007). Craniofacial variability index determined by three-dimensional ultrasound in isolated vs. syndromal fetal cleft lip/palate. Ultrasound Obstet Gynecol 29:265–70.

Rotten D, Levaillant JM (2004). Two- and three-dimensional sonographic assessment of the fetal face. 1. A systematic analysis of the normal face. Ultrasound Obstet Gynecol 23:224-31.

Sepulveda W, Wong AE, Martinez-Ten P, Perez-Pedregosa J (2010). Retronasal triangle: a sonographic landmark for the screening of cleft palate in the first trimester. Ultrasound Obstet Gynecol 35:7–13.

Tonni G, Lituania M (2012). OmniView Algorithm — A Novel 3-Dimensional Sonographic Technique in the Study of the Fetal Hard and Soft Palates. J Ultrasound Med 31:313–8.

Tonni G, Lituania M (2013). Arthrogryposis multiplex congenita-like syndrome associated with median cleft lip and palates: First prenatally detected case. Congenital Anomalies 53:13–40.

Vezzetti E, Marcolin F (2012). 3D human face description: landmarks measures and geometrical features. Image and Vision Computing 30(10):698-712.

Vezzetti E, Marcolin F (2012). Geometrical descriptors for human face morphological analysis and recognition. Robotics and Autonomous Systems 60(6):928-39.

Vezzetti E, Marcolin F (2012). Geometry-based 3D face morphology analysis: soft-tissue landmark formalization. Multimedia Tools and Applications 68(3):895-929.

Vezzetti E, Marcolin F (2014). 3D Landmarking in Multiexpression Face Analysis: A Preliminary Study on Eyebrows and Mouth. Aesthetic Plastic Surgery 38(4):796-811.

Vezzetti E, Calignano F, Moos S (2010). Computer-aided morphological analysis for maxillo-facial diagnostic: a preliminary study. Journal of Plastic, Reconstructive & Aesthetic Surgery 63(2):218-26.

Vezzetti E, Marcolin F, Fracastoro G (2014). 3D face recognition: An automatic strategy based on geometrical descriptors and landmarks. Robotics and Autonomous Systems 62(12):1768-76.

Vezzetti E, Marcolin F, Stola V (2013). 3D Human Face Soft Tissues Landmarking Method: An Advanced Approach. Computers in Industry 64(9):1326–54.

Vezzetti E, Moos S, Marcolin F (2011). Three-Dimensional Human Face Analysis: Soft Tissue Morphometry. Proceedings of the InterSymp 2011. Baden-Baden, Germany.

Vezzetti E, Moos S, Marcolin F, Stola V (2012). A pose-independent method for 3D face landmark formalization. Computer Methods and Programs in Biomedicine 198(3):1078-96.

Vezzetti E, Speranza D, Marcolin F, Fracastoro G (2014). Exploiting 3D Ultrasound for Fetal Diagnosis Purpose through Facial Landmarking. Image Analysis & Stereology 33(3):167-88.

APPENDIX

The First and Second Fundamental Forms are used to measure distance on surfaces and are defined by

$$E\,du^2 + 2F\,du\,dv + G\,dv^2 , \quad (1)$$

$$e\,du^2 + 2f\,du\,dv + g\,dv^2 , \quad (2)$$

respectively, where *E*, *F*, *G*, *e*, *f* and *g* are their Coefficients. Curvatures are used to measure how a regular surface *x* bends in R^3. If *D* is the differential and *N* is the normal plane of a surface, then the determinant of *DN* is the product $(-k_1)(-k_2) = k_1 k_2$ of the Principal Curvatures, and the trace of *DN* is the negative $-(k_1 + k_2)$ of the sum of Principal Curvatures. In point *P*, the determinant of DN_P is the *Gaussian Curvature K* of *x* at *P*. The negative of half of the trace of *DN* is called the *Mean Curvature H* of *x* at *P.* In terms of the principal curvatures can be written

$$K = k_1 k_2 , \quad (3)$$

$$H = \frac{k_1 + k_2}{2} .$$

(4)

Some definitions of these descriptors are given. These are the forms implemented in the algorithm:

$$E = 1 + h_x^2 \ , \tag{5}$$

$$F = h_x h_y \ , \tag{6}$$

$$G = 1 + h_y^2 \ , \tag{7}$$

$$e = \frac{h_{xx}}{\sqrt{1 + h_x^2 + h_y^2}} \ , \tag{8}$$

$$f = \frac{-h_{xy}}{\sqrt{1 + h_x^2 + h_y^2}} \ , \tag{9}$$

$$g = \frac{-h_{yy}}{\sqrt{1 + h_x^2 + h_y^2}} \ , \tag{10}$$

$$K = \frac{h_{xx} h_{yy} - h_{xy}^2}{\left(1 + h_x^2 + h_y^2\right)^2} \ , \tag{11}$$

$$H = \frac{\left(1 + h_x^2\right) h_{yy} - 2 h_x h_y h_{xy} + \left(1 + h_y^2\right) h_{xx}}{\left(1 + h_x^2 + h_y^2\right)^{3/2}} \ , \tag{12}$$

$$k_1 = H + \sqrt{H^2 - K} \ , \tag{13}$$

$$k_2 = H - \sqrt{H^2 - K} \ , \tag{14}$$

where h is a differentiable function $z=h(x,y)$. It is, therefore, convenient to have at hand formulas for the relevant concepts in this case. To obtain such formulas let us parametrize the surface by

$$x(u,v)=(u,v,h(u,v)) , \qquad (u,v)\in U , \tag{15}$$

where $u = x$, $v = y$.

The most used descriptors are surely the Shape and Curvedness Indexes S and C, introduced by Koenderink *et al.*[1]:

$$S=\frac{-2}{\pi}\arctan\frac{k_1+k_2}{k_1-k_2} , \qquad S\in[-1,1] , \qquad k_1\geq k_2 , \tag{16}$$

$$C=\sqrt{\frac{k_1^2+k_2^2}{2}} . \tag{17}$$

For the role they play in the work, a little digression about their significance is needed. Their meaning is shown in Figures 19-21 and in Table 5.

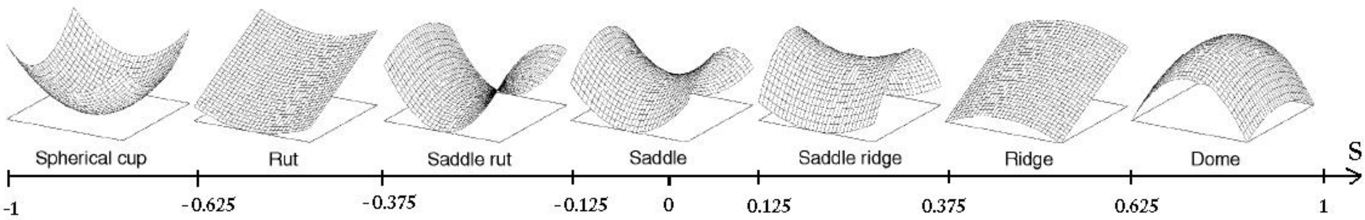

Figure 19. Illustration of Shape Index scale divided into seven categories. Different subintervals of its range [-1,1] correspond to seven geometric surfaces.

Class	***S***	**Type**	***H***	***K***
cup/pit	[-1,-0.625)	elliptical convex	+	+
rut/valley	[-0.625,-0.375)	cylindrical convex	+	0
saddle rut/saddle valley	[-0.375,-0.125)	hyperbolic convex	+	-
saddle	[-0.125,0.125)	hyperbolic symmetric	0	-
saddle ridge	[0.125,0.375)	hyperbolic concave	-	-
ridge	[0.375,0.625)	cylindrical concave	-	0
dome/peak	[0.625,1)	elliptical concave	-	+

Table 5. Topographic classes.

[1] Koenderink, J.J. and van Doorn, A.J., 1992. Surface shape and curvature scales. Image and Vision Computing 10(8), 557-564.

Figure 20. Curvedness Index scale, whose range is $(-\infty, \infty)$.

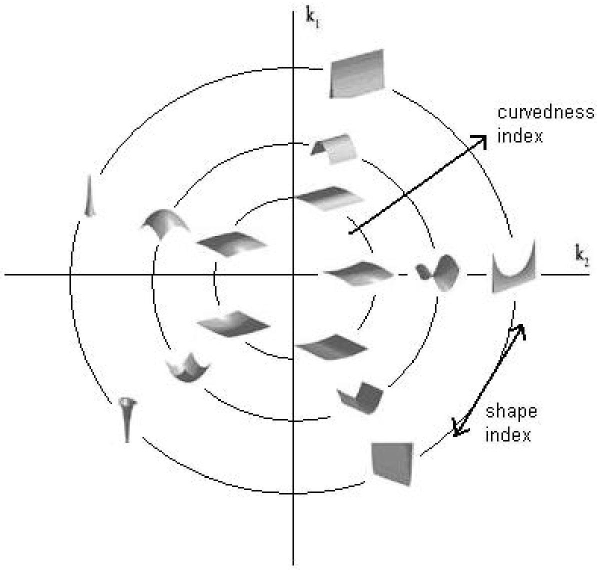

Figure 21. Indexes (*S*,*C*) are viewed as polar coordinates in the (k_1, k_2) -plane, with planar points mapped to the origin. The effects on surface structure from variations in the curvedness (radial coordinate) and Shape Index (angular coordinate) parameters of curvature, and the relation of these components to the principal curvatures (k_1 and k_2). The degree of curvature increases radially from the centre.